
xTrimoGene: An Efficient and Scalable Representation Learner for Single-Cell RNA-Seq Data

Jing Gong^{1*} Minsheng Hao^{12*} Xingyi Cheng^{1†} Xin Zeng¹
 Chiming Liu¹ Jianzhu Ma² Xuegong Zhang² Taifeng Wang¹ Le Song^{13†}

¹ BioMap Research ² Tsinghua University

³ Mohamed bin Zayed University of Artificial Intelligence

{gongjing, minsheng_2022, xingyi, zengxin, chiming, taifeng, songle}@biomap.com,
 {zhangxg, majianzhu}@tsinghua.edu.cn

Abstract

Advances in high-throughput sequencing technology have led to significant progress in measuring gene expressions at the single-cell level. The amount of publicly available single-cell RNA-seq (scRNA-seq) data is already surpassing 50M records for humans with each record measuring 20,000 genes. This highlights the need for unsupervised representation learning to fully ingest these data, yet classical transformer architectures are prohibitive to train on such data in terms of both computation and memory. To address this challenge, we propose a novel asymmetric encoder-decoder transformer for scRNA-seq data, called xTrimoGene^α (or xTrimoGene for short)⁴, which leverages the sparse characteristic of the data to scale up the pre-training. This scalable design of xTrimoGene reduces FLOPs by one to two orders of magnitude compared to classical transformers while maintaining high accuracy, enabling us to train the largest transformer models over the largest scRNA-seq dataset today. Our experiments also show that the performance of xTrimoGene improves as we scale up the model sizes, and it also leads to SOTA performance over various downstream tasks, such as cell type annotation, perturb-seq effect prediction, and drug combination prediction. xTrimoGene model is now available for use as a service via the following link: <https://api.biomap.com/xTrimoGene/apply>

1 Introduction

Recently, Artificial Intelligence (AI) technology has demonstrated promising results for addressing scientific problems. This AI4Science paradigm witnessed diverse successful biological and pharmaceutical applications, including protein analysis [Jumper et al., 2021, Lin et al., 2023, Zhang et al., 2022, Xiao et al., 2021, Brandes et al., 2022], RNA modeling [Chen et al., 2022a], and genomics modulation [Pesaranhader et al., 2022]. However, most existing AI models have predominantly focused on protein sequences, neglecting the growing volume of high-throughput experimental sequencing data in the form of gene expression values. Single-cell RNA sequencing (scRNA-seq) technology has transformed the field of cell biology and enabled us to understand cell-cell, cell-gene and gene-gene relations at the cellular level [Jovic et al., 2022, Chen et al., 2019]. This technique captures the expression levels of thousands of genes in parallel, facilitating the study of cellular heterogeneity

*Equal contribution. Mingsheng Hao conducted this work during his internship at BioMap.

†Correspondence to: xingyi@biomap.com, songle@biomap.com.

⁴xTrimoGene is a member of BioMap’s large-scale AI engine "xTrimo" series. "α" denotes the academic version, to distinguish it from the commercial product xTrimoGene. The code has been merged into the ScFoundation repository, which is available at <https://github.com/biomap-research/scFoundation>.

[Chen et al., 2022b, Li et al., 2022]. This unveiled information is crucial for understanding complex biological systems and disease progression [Jovic et al., 2022, Chen et al., 2019]. Integrating and modeling such large-scale scRNA-seq data can reveal rich cellular information and benefit various biological task learning.

Representation learning from scRNA-seq data [Flores et al., 2022] has been an active area of research in past decades. For example, scVAE [Grønbech et al., 2020] and scVI [Lopez et al., 2018] apply a variational autoencoder framework to derive low-dimensional cell embeddings, cscGAN [Marouf et al., 2020] uses a Generative Adversarial Network (GAN) architecture to generate cell-type specific expression profiles, and SAVER-X [Wang et al., 2019] is capable of removing batch effects across datasets. Despite the success of these customized algorithms, they tend to be computationally inefficient and labor-intensive. This prompts us to explore a general-purpose model that first learns underlying knowledge from scRNA-seq data and generalizes it to different tasks in a unified manner. We draw inspiration from the pre-training and fine-tuning paradigm in Natural Language Processing (NLP), which has shown great success in improving various downstream NLP task performance [Qiu et al., 2020, Han et al., 2021, Hendrycks et al., 2019]. In light of these findings, we aim to investigate the potential of applying similar approaches to representation learning in scRNA-seq data.

The first published pre-trained model for single-cell data is scBERT, which uses a low-rank transformer [Yang et al., 2022] to analyze the scRNA data. It learns the cellular representation by randomly masking a percent of non-zero gene expression values and tries to recover them. scBERT has achieved state-of-the-art results for cell-type annotation tasks. The study shows the potential of a pre-training strategy for single-cell biology research. However, scBERT has certain limitations in fully utilizing scRNA-seq data properties. These limitations include:

(1) Scalability. The large number of genes (almost 20,000) and the sparsity of scRNA-seq data, with nearly 90% of values being zero, lead to many redundant computations (e.g., self-attentions between zero tokens). It required approximately 2.65×10^{19} FLOPs to train 5 million samples over 5 epochs, which equals almost 20 days of training on an A100 GPU for only an 8.9 million parameter scBERT model. (2) Limited resolution for expression values. scBERT rounds the gene expression values into integer values, which limits the model’s ability to distinguish closeness and similarity between gene expression values. For instance, two close values could be mapped to separate embeddings (e.g., 1.99 and 2.01 are mapped to 1 and 2), and two distant values could be mapped to identical embeddings (e.g., 1.99 and 1.01 are mapped to 1). The strategy leads to a loss of resolution and introduces bias during model training, resulting in sub-optimal performance.

To address the challenges associated with scRNA-seq data modeling and consider the unique nature of this data (as discussed in Section 2), we present a novel and efficient framework, xTrimoGene, for pre-training large-scale scRNA-seq data. Our framework makes the following key contributions:

- (1) We design an asymmetrical encoder-decoder architecture to guide the pre-training process, which enables us to learn a high-capacity model for single-cell RNA-seq data. Our model achieves an improvement in the speed of pre-training of over 3 times compared to previous encoder-only models.
- (2) We illustrate that the efficiency and scalability of our model allow us to train the largest single-cell pre-trained model to date, with approximately 100 million parameters for the xTrimoGene-100M model, using a curated scRNA-seq dataset of approximately 50 billion effective gene tokens.
- (3) The pre-trained model xTrimoGene achieved remarkable results in multiple downstream tasks, including cell type annotation, perturbation prediction and synergistic drug combination prediction.

2 Characteristics of Single-Cell RNA-seq Data

scRNA-seq generates a large, sparse expression matrix, where each row represents a cell (sample) and each column a gene (feature). This dataset presents several challenges and requires a specialized architecture to effectively model the data.

First, approximately 20,000 genes (columns) are shared across cells. Unlike the corpus in NLP, the genes can be arbitrarily reordered. The relation between genes depends on biological pathways rather than local contexts, where the latter shapes spatial information in Computer Vision (CV) images. Though one can roughly regard each cell (row) as a sentence or an image patch, the 20,000 genes is a vast number compared to the typical sequence length, which is mostly a few hundred and no more

than a few thousand [Qiu et al., 2020, Han et al., 2021]. Thus directly applying existing transformer architecture will not work.

Second, scRNA-seq matrices are highly sparse (90% zero in a typical dataset [Jiang et al., 2022, Ding et al., 2020]). The abundance level of RNA for each gene is measured by counting the unique molecular identifier (UMI) reads in scRNA-seq experiments [Jovic et al., 2022, Chen et al., 2019]. However, many genes exhibit low UMI counts due to limited probing efficiency. Therefore, treating scRNA-seq data as an image and utilizing a convolutional neural network to extract features is not feasible, as it introduces a huge number of redundant computations for sparse positions.

Third, the normalized gene expression values in scRNA-seq data are continuous scalars, which typically indicate similar gene activity when they have similar values. To transform these scalars into high-dimensional tokens in the data matrix, a representation that preserves the continuous semantics is needed. Manually discretizing the gene expression values is challenging as non-optimal discretization thresholds will bias category assignment. A learned discretization approach or learnable representation, such as the one proposed in [Gorishniy et al., 2022], is ideal for preserving the continuous semantics of the gene expression values.

Taking into the above three major features, we design a new architecture as described in the next section.

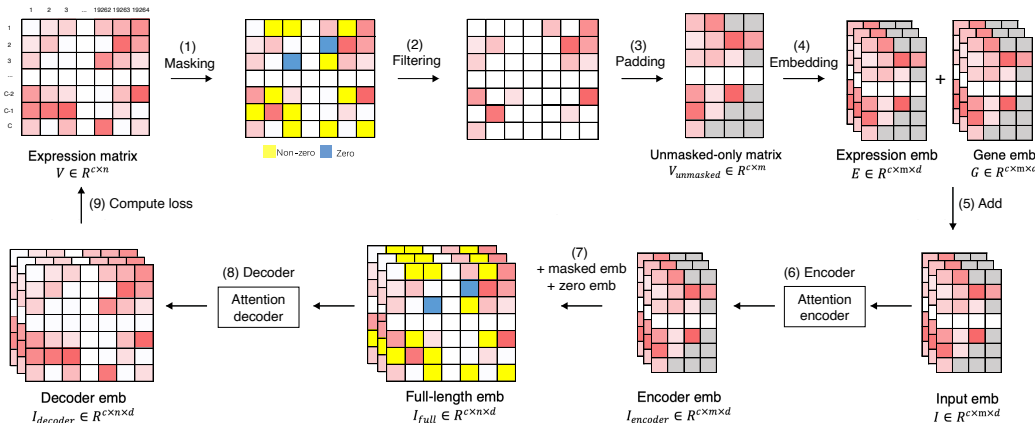


Figure 1: The xTrimoGene Framework: (1) Random positions (including both zero and non-zero values) are masked for prediction. (2) Masked and zero-valued positions are filtered out. (3) Remaining unmasked positions are aligned with padding tokens (grey) to ensure maximum length consistency within a batch. (4) Gene expression values and gene embeddings are separately projected into embeddings. (5) These two embeddings are element-wise added. (6) The resulting input is fed into the encoder. (7) The intermediate encoder embedding is combined with embeddings for masked positions and zero embeddings. (8) This combined representation is then fed into the decoder. (9) Decoder embedding is projected to model output with an MLP layer. The MSE loss is calculated between the model output and ground truth values for the masked positions.

3 xTrimoGene Architecture

xTrimoGene is a highly efficient framework for pre-training large-scale single-cell RNA-seq data (illustrated in Figure 1). The training process is based on a regression-masked task, aimed at accurately recovering masked values in the expression matrix. Notably, a specific optimized asymmetrical encoder-decoder framework is employed to accelerate the learning of sparse matrices. This is achieved by feeding only the unmasked non-zero positions (less than 10% of the full length) into the encoder, while the largely masked and zero positions are input into a lightweight decoder with a reduced number of layers and attention heads. In addition, a novel auto-discretization strategy is introduced to project continuous expression values into a latent embedding space. Instead of rounding to the nearest integer, values are directly mapped to the latent space allowing for the representation of closely related values. The xTrimoGene framework consists of the following components:

Masking: A portion of the normalized gene expression matrix V is masked for prediction, including both zero and non-zero positions. c denotes cell sample size, and n denotes gene number (19,264 in our setting, see App. 1 for data collection and processing).

Filtering: The masked and zero-valued embeddings are filtered out, yielding a variable-length sequence of valuable information that is prepared for encoding.

Padding: The remaining unmasked positions are aligned with padding tokens, resulting in a much smaller unmasked-only matrix $V_{unmasked}$. m denotes the maximum length of the unmasked sample. We include a scheme to illustrate the processing flow (see App. 2).

Embedding: Expression value and gene embeddings are separately projected. d denotes the dimension of the embedding. The expression embedding is calculated through an auto-discretization mapping. The gene embedding is retrieved from a randomly initialized lookup table.

Combining Expression and Gene Embeddings: The expression and gene embeddings (E and G) are element-wise added to form the input embedding, which is then fed into the encoder of the model.

Encoding: The sum of the embeddings is input into the encoder, which implements self-attention mechanisms using a Transformer-like architecture.

Extending masked and zero embeddings: The intermediate encoder embedding $I_{encoder}$ is combined with embeddings for masked and zero-value positions.

Decoding: The combined embeddings are processed by the decoder, utilizing self-attention mechanisms instead of the typical casual attention used in NLP decoders.

Loss Computation: Decoder embedding is projected to model output with an MLP layer. The mean squared error (MSE) loss is computed between the predicted masked values from the model and their corresponding ground truth values.

3.1 Encoder

The scRNA-seq data is characterized by its high sparsity, with cell information largely concentrated in the non-zero expression values. Thus, the encoder is designed to focus only on the non-zero part of the unmasked matrix, $V_{unmasked}$. The encoder is based on a traditional multi-head attention transformer and takes the combination of value embedding, E , and gene embedding, G , as its input, $I \in \mathbb{R}^{c \times m \times d}$. The value and gene embeddings are similar to the word and positional embeddings in natural language modeling, respectively. The value embedding, E , is generated using the auto-discretization strategy discussed previously, while the gene embedding, G , is retrieved from a function f_L that maps the gene symbols into the embedded vocabulary.

$$E = \text{Autobin}(V_{unmasked} \odot M_{nonzero}), G = f_L(\text{genes}), I = E + G \quad (1)$$

Then the encoder processes the input embeddings I and generates the high-level gene representations $I_{encoder} \in \mathbb{R}^{b \times m \times d}$ via the multi-head attention mechanism.

$$I_{encoder} = \text{Trm}(f_Q(I), f_K(I), f_V(I)) \quad (2)$$

where f_Q, f_K, f_V are the project functions. Trm denotes the Transformer block.

It is worth emphasizing that our encoder only operates on a subset of genes, reducing the length of the processed sequence to 1/10 of the original. This allows the full-length transformer to be used without any computational approximations.

3.2 Decoder

Unlike the encoder which focuses on the main information (non-zero expression values) in the cells, the decoder in the system performs full-length feature abstraction and extraction. The input to the decoder, I_{full} , comprises three token types: the output from the encoder, $I_{encoder}$, the genes with zero expression embs I_{zero} , and the mask token embs I_{masked} . Out of these tokens, genes with zero expression make up 90% of all tokens. The gene embeddings are concatenated with all of these tokens to provide the decoder with gene-specific information for the corresponding mask tokens, followed by a full connection layer.

$$I_{full} = W_p(I_{encoder} \oplus I_{zero} \oplus I_{masked}) + b_p \quad (3)$$

where \oplus represents the concatenation operation, and W_p and b_p are learnable parameters that project the decoder’s embedding size.

The decoder in the framework is optimized for long-sequence attention calculations and employs the Performer architecture as its backbone. The decoder transforms the input I_{full} into final gene-level embeddings, $I_{decoder} \in \mathbb{R}^{b \times n \times d}$, and predicts the masked values through a shared linear layer, $W \in \mathbb{R}^{d \times 1}$, applied across all genes. The operations are expressed as follows:

$$I_{decoder} = \text{Trm}((f_Q(I_{full}), f_K(I_{full}), f_V(I_{full})), \tilde{V} = I_{decoder} \cdot W \quad (4)$$

The decoder has a smaller model size compared to the encoder, with a smaller embedding size, fewer attention layers, and fewer attention heads. For instance, in the largest model configuration, the layer depth ratio between the encoder and decoder is 2:1 and the head number ratio is 1.5:1 (see App. Table 2). Similarly, the principle of asymmetric encoder-decoder design has been proven powerful in masked autoencoders (MAE) [He et al., 2022], which is tailored for CV data pre-training. Unlike MAE, xTrimoGene utilizes the biased masking strategy to avoid the learning process being dominated by zero tokens. Though the scRNA-seq data is distinct from images, our results show that the performance gains of xTrimoGene are comparable to those of MAE, with more efficient training and better downstream task performance.

3.3 Auto-discretization strategy

Our aim is to transform an expression value v into a hidden embedding, denoted as e . The transformation is achieved using an auto-discretization block. This auto-discretization process involves a random look-up table T defined in $\mathbb{R}^{d \times b}$. In this representation, d refers to the embedding dimension, while b is the number of bins with a default value of 100. The transformation starts by applying a linear layer to the expression value, given by $v_1 = v \cdot w_1$, where w_1 represents the weight vector. The resulting v_1 is then subjected to a leaky ReLU activation, resulting in $v_2 = \text{Leaky_ReLU}(v_1)$. Subsequently, a cross-layer projection is applied, represented by $v_3 = w_2 \cdot v_2 + \alpha \cdot v_2$. Here, w_2 denotes the weight vector, and α is a scaling mixture factor. Next, the bin weights of v_3 are normalized using the softmax function, resulting in $v_4 = \text{softmax}(v_3)$. Finally, the transformed value is represented as a weighted combination of individual embeddings from the look-up table, given by $e = T \cdot v_4$. It’s important to note that the weights in this combination serve as learnable parameters.

To validate the effectiveness of the expression value projection, we conducted an analysis of viewing the weight distribution pattern for continuous values. Our results showed that the normalized weight distribution of the close values exhibited smooth transitions and that of the distant values being clearly distinguishable (App. section 3 Figure 1). This supports the conclusion that the auto-discretization strategy effectively represents continuous values with high resolution while preserving relatively rich meaning.

We also compared the performance of the proposed auto-discretization strategy with three other discretization methods: (1) Round bin with zero, in which values are rounded to the nearest integer, and zeros are kept as it is, (2) Up bin without zero. Values greater than zero are converted to the nearest ceiling integer, while zero is represented as individual 0. (3) Equal bin. All the values fall into a fixed percentage interval, which is calculated by value distribution and frequency. We evaluated the different strategies on a standard cell clustering task (see App. 4) and found that the proposed auto-discretization strategy outperformed the others (as shown in Figure2 A), demonstrating the importance of high-resolution projections in handling expression values.

4 Training Strategy

We now explain the strategy used to train the asymmetric encoder-decoder transformer. Pre-trained task and masking strategy are outlined, see App. 5 for acceleration strategy.

4.1 Regression masked task

The traditional masked language task is a multi-class classification problem, where the predicting target is a single token with limited, naturally distinct categories. In contrast, the normalized gene

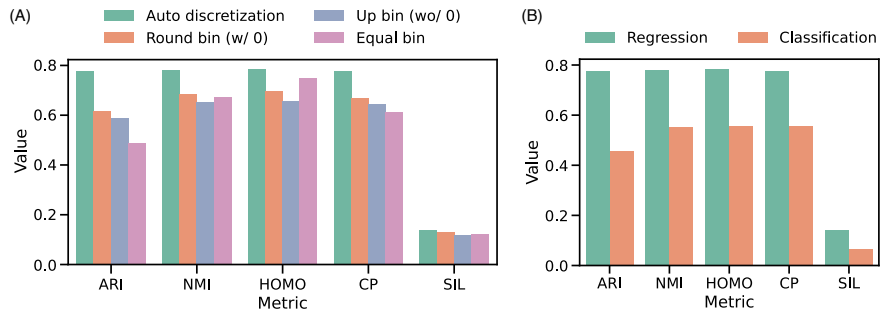


Figure 2: Pre-training strategy ablation study. (A) Performance comparison between auto discretization strategy and other binning methods for expression value projection. The cell clustering task is evaluated and five metrics are displayed. ARI for Adjusted Rand index, NMI for Normalized Mutual Information, HOMO for Homogeneity, CP for Completeness and SIL for Silhouette Coefficient. (B) Performance of pre-trained models with different task modes, including regression and classification settings. The cell clustering task is evaluated. See the main text for details.

expression value is a continuous scalar. To fit the data property, we modify the pre-trained learning objective to a regression task, aimed at recovering the absolute value of the masked positions. The loss function employed is the MSE between the ground truth and the predicted values:

$$\text{Loss} = \frac{1}{(n - m) * c} \sum (V_{i,j} - \tilde{V}_{i,j})^2 \quad (5)$$

where n represents the number of all genes, m represents the maximum length of the unmasked positions in a sample, and c represents the number of cells. To evaluate the efficacy of this modification, we compared the regression setting with the classification setting on the cell clustering task. The results indicate that the regression model outperforms the classification model (Figure 2B), providing evidence of the benefits of learning a more fitted representation.

4.2 Masking strategy

We mask both non-zeros and zeros positions though the scRNA-seq expression matrix is highly sparse (where zero percentage is usually over 90%). As the zero positions percentage is much higher than non-zero positions, the masked ratio can't be the same for the two types. Otherwise, the model tends to predict all zeros and still obtains a low error level. We propose to mask an almost equal number of positions for zero and non-zeros positions (see App. section 6 Table 1). The setting enforces the model to learn embeddings for all values and not to be dominated by zero representation. We found zero values supervision is necessary to boost the performance (App. Figure 2), which demonstrates that some zeros represent the true extremely low expression level. This type of zeros is informative to illustrate how the gene abundant behaves inside the cell.

The recovery of masked tokens in NLP is challenging due to the fact that word comprehension relies heavily on long-range interactions rather than local context. Accurate inference of the missing tokens can be achieved at low masking ratios (15%) where the information in the entire sentence is still relatively redundant and encoded by the unmasked tokens. We investigated the density of information needed for the scRNA-seq regression task by training models with different masking ratios (for non-zero values, the ratio was set 10 times higher than for zero values) ranging from 15% to 90% with a 15% interval. The models were then evaluated on the cell clustering task, with the results showing that performance improved first and then degraded as the masking ratio increased. When the masking ratio was close to 30%, the majority of metrics reached a peak (App. Figure 3). We also found current biased masking is optimal (App. Figure 4) and the percentage of [MASK] tokens agrees well with NLP tasks (App. Figure 5). These results suggest that the scRNA-seq expression vector contains more redundant information than a sentence and highlight the role of hidden regulations between genes in constraining the inference of expression values.

5 Experiments

Next we will explain our experimental settings and results. The dataset description can be referred to App. 1.

5.1 Computational efficiency

We quantitatively compared the training cost of xTrimoGene with other two encoder-only models, including full-length attention Transformer and kernel-based approximation Performer (scBERT). For an apple-to-apple comparison, three models are set to approximately 10 million trainable parameters and trained on 5 million samples over 5 epochs. We calculated the corresponding FLOPs, where matrix multiplication operations are considered only. We observed that total FLOPs for Performer (scBERT) decreased to 10% of native Transformer (see Table 1). Notably, xTrimoGenes runs 3-times faster than Performer. The results validate the efficiency of xTrimoGene, which is readily adapted for large-scale data pre-training.

Table 1: Computational efficiency comparison between different algorithms. The resource column is normalized by the Transformer row.

Model name	Parameter (M)	Forward + backward (FLOPs/sample)	Total train (FLOPs)	Resource
Transformer	11.3	9.86E+12	2.46E+20	100%
Performer	8.9	1.06E+12	2.65E+19	10.8%
xTrimoGene	9.8	3.35E+11	8.38E+18	3.4%

5.2 Scalability

The Deep Learning community has shown significant interest in the scalability of proposed models [Kaplan et al., 2020, Brown et al., 2020]. Vanilla Transformer models are challenging to scale due to their computational time and resource requirements, which increase quadratically with model size. Varieties of attention mechanisms have been proposed to accelerate training speed, a critical factor for model scaling.

To test the scale-up ability of xTrimoGene, we pre-trained three models across multiple compute regions and scales (e.g., from 3M to 100M parameters). The detailed hyperparameter setting is displayed in the App. Table 2. The training curve clearly shows all models are steadily down to a lower loss when training steps increase (App. Figure 6). More importantly, the xTrimoGene-100M model obtains a significant improvement over the xTrimoGene-10M model, which is also superior to the xTrimoGene-3M model. The tendency is consistent across different data sizes. The results suggest xTrimoGene framework is robust to scale-up, making it possible and convenient to pre-train larger models with more data.

5.3 Robustness on high sparse data

scRNA-seq data often exhibit varying levels of sparsity, thus it's necessary to assess whether xTrimoGene is robust in handling different sparse data. To verify the robustness, we divided the test samples into subgroups based on cell type and calculated the sparsity level (i.e., percentage of zero values in the expression matrix) and Pearson correlation coefficient between the predicted and actual values. Our results reveal that the correlation gradually decreases as the sparsity level increases, as expected (Figure 3A). However, the correlation remains above 0.8 even when the sparsity level reaches 96% (Figure 3A), indicating the robustness of xTrimoGene. We also compared xTrimoGene's performance with Performer and found that xTrimoGene consistently achieves a higher correlation across most subgroups (Figure 3B). These findings demonstrate that xTrimoGene is robust in handling highly sparse data and outperforms encoder-only architectures.

The performance of the encoder-decoder and encoder-only architectures have been comparatively analyzed in the NLP domain, with the former demonstrating effectiveness in language comprehension and the latter in context generation. Apart from comparison on masked value recovery, we further

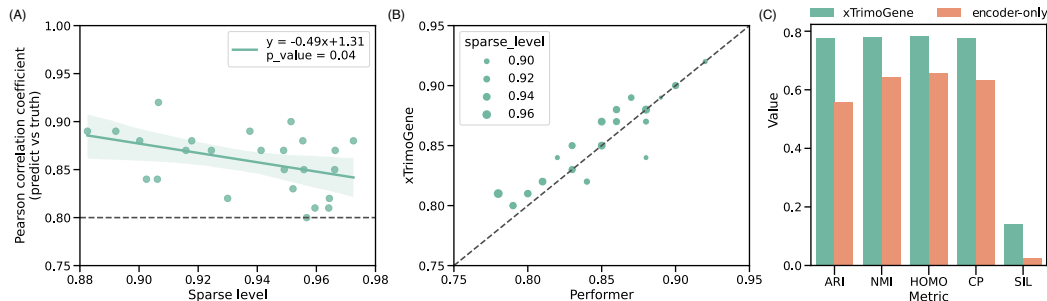


Figure 3: Comparison of performance for different sparse level data. (A) xTrimoGene performance for recovering masked values at different sparse levels. Each dot represents a subset defined by cell type. Sparse level is calculated as the ratio between zero value percentages. Pearson correlation coefficient metric is calculated on masked positions. (B) Performance comparison of xTrimoGene and Performer while recovering masked values at different sparse levels. Dot has the same meaning as (A) but the dot size is proportional to the sparse level. Both the x and y axis denotes the Pearson correlation coefficient metric for a particular algorithm. (C) Comparison of performance for xTrimoGene framework and encoder-only framework. Cell clustering task is evaluated.

evaluated xTrimoGene against encoder-only Performer on the cell clustering task. The results demonstrate that xTrimoGene achieves superior performance, reaffirming its proficiency in latent embedding extraction (Figure 3C).

5.4 Evaluation on downstream tasks

Currently, multiple tasks have been established to evaluate different models, including well-defined cell type annotation and recently developed perturbation response prediction tasks. We first assessed the performance of xTrimoGene on these single-cell tasks. Additionally, we explored the potential application on bulk RNA-sequencing data, with a focus on synergistic drug combination prediction.

5.4.1 Cell type annotation

First, we evaluated xTrimoGene’s performance on cell type annotation task with Zheng68K [Zheng et al., 2017] and Segerstolpe [Segerstolpe et al., 2016] dataset, which has been widely benchmarked. We compared the xTrimoGene against other several methods, including scBERT [Yang et al., 2022], ACTINN [Ma and Pellegrini, 2020], Scanpy [Wolf et al., 2018], CellTypist [Conde et al., 2022], scVI [Lopez et al., 2018] and singleCellNet [Yuqi Tan, 2019]. For the xTrimoGene model, we added a max-pooling layer and a linear layer to predict cell type labels with fine-tuning mode (see App. 8.1). For other methods, we followed their instruction with the default parameter setting. We observed that xTrimoGene achieves a high Precision and F1 score, surpassing all the other methods (Table 2). The results indicated that xTrimoGene learns a well-represented cellular embedding (visualized in App. Figure 7) by simply aggregating contextual gene embedding.

Table 2: The cell annotation performance on the Zheng68K and Segerstolpe dataset. xTrimoGene is evaluated with 100M parameter model.

Method Name	Zheng68K		Segerstolpe	
	Precision	F1 score	Precision	F1 score
xTrimoGene	0.7335 ± 0.0226	0.7354 ± 0.0189	0.8112 ± 0.0009	0.8140 ± 0.0008
scBERT	0.7029 ± 0.0115	0.6695 ± 0.0077	0.6818 ± 0.0736	0.6703 ± 0.0653
ACTINN	0.6720 ± 0.0021	0.6486 ± 0.0041	0.7545 ± 0.0018	0.7219 ± 0.0073
Scanpy	0.6111 ± 0.0017	0.5474 ± 0.0085	0.6274 ± 0.0000	0.5398 ± 0.0000
CellTypist	0.7454 ± 0.0009	0.7151 ± 0.0038	0.7923 ± 0.0003	0.8117 ± 0.0001
scVI	0.4883 ± 0.0005	0.4843 ± 0.0008	0.5101 ± 0.0022	0.5208 ± 0.0016
singleCellNet	0.6452 ± 0.0013	0.5982 ± 0.0027	0.7551 ± 0.0096	0.8055 ± 0.0076

5.4.2 Perturbation response prediction

Recently, perturb-seq technology was established to screen gene expression response given pooled perturbations at single-cell level [Dixit et al., 2016]. Several algorithms have also been developed to predict perturbation effects [Roohani et al., 2022, Lotfollahi et al., 2021] at the single cell level, i.e., what is the expression value of genes after perturbation? We compared the native GEARs [Roohani et al., 2022] model with and without incorporating embeddings from xTrimoGene.

The normal state (before perturbation) gene expression profile is fed into xTrimoGene and we obtained the context embedding, which replaces raw expression value input in the GEARs model (App. 8.2). All the other settings remain unchanged. The evaluated dataset (Norman et al. [Norman et al., 2019]) contains both single and double gene perturbation and we thus assess the performance across different perturbation levels. As shown in Figure 4A, GEARs with xTrimoGene embedding scores a lower MSE (decreased 14.8%) for top20 differential expressed genes across all perturbation scenarios. Notably, the tendency is consistent across different perturbation levels, regardless the perturbed target is seen or not. We also compared against the scBERT embedding and observed a similar trend, where xTrimoGene achieves better results (App. Table 3). The results demonstrated that the pre-training strategy empowers xTrimoGene to capture constraints under various circumstances, including post-perturbations. The application further proved the efficacy and potential of xTrimoGene to boost scRNA-seq based tasks.

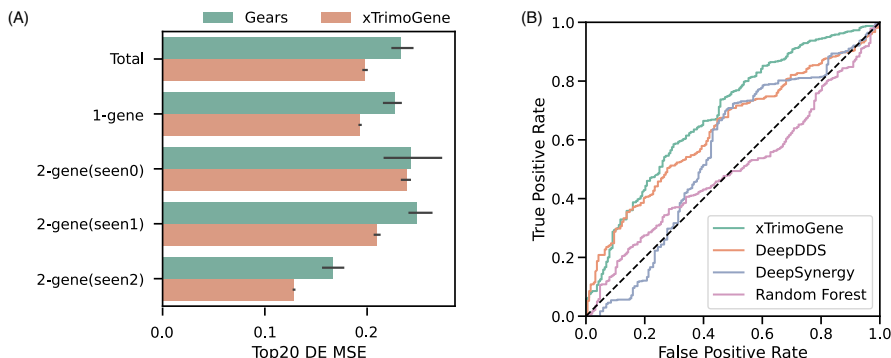


Figure 4: (A) The MSE of the top 20 differentially expressed (DE) genes given by different models on perturbation response prediction. The top 20 DE genes are calculated between the before and post-perturbation expression profiles. "Total" denotes evaluating all test perturbation sets. "1-gene" denotes evaluation on the single gene perturbation subset, where the perturbed target is not seen in the training set. "2-gene" represents the sub-test set for perturbing two genes simultaneously. "seen0", "seen1" and "seen2" denotes zero, one or two perturbed targets are not seen in the training set, respectively. The black line denotes a 95% confidence interval. (B) ROC curve of different models on drug combination synergy prediction task. xTrimoGene denotes replacing the raw expression profile with context embeddings in the DeepDDS framework and others remain unchanged. Refer to App. 8.3 for more details.

5.4.3 Synergistic drug combinations prediction

The drug synergistic task evaluates how patients or cells respond to a drug combination intervention [Mokhtari et al., 2017]. However, the generated wet-lab experimental data only covers a tiny search space of possible drug combinations. Multiple models have been proposed to accelerate predicting the synergistic landscape of drugs [Preuer et al., 2017, Wang et al., 2022]. For instance, DeepDDS integrates genomic expression profiles and drug chemical information, greatly improving the prediction performance. We further explored whether xTrimoGene is able to generate good latent embedding for this bulk expression data.

Similar to the perturbation prediction test, we adapted xTrimoGene to DeepDDS with the intermediate context embedding (see App. 8.3). We also included DeepSynergy and Random Forest for comparison. As illustrated in Figure 4B, utilizing embedding from the xTrimoGene model outperforms all the other models. The result proved that xTrimoGene can accurately capture cell-level representation,

even for bulk sequencing data. This also opens the avenue for xTrimoGene to be applied across other biological modeling tasks, especially where bulk-level transcriptome data is available.

6 Conclusion

xTrimoGene is a new, efficient framework for learning scRNA-seq data. It proposes an asymmetric encoder-decoder framework that takes advantage of the sparse gene expression matrix and establishes the projection strategy of continuous values with a higher resolution. The results show that xTrimoGene is scalable and performs well on tasks like cell type annotation, perturbation response prediction, and synergistic drug combination prediction. The experiments demonstrate the efficacy of pre-training in single-cell biology. xTrimoGene is potentially adapted to other types of cell modeling analysis, including rare cell detection (App. 8.4), batch effect removal and regulatory network construction.

Certain limitations exist for xTrimoGene and further work is desired to advance the design. At present, xTrimoGene majorly utilizes gene expression values during the pre-training stage, overlooking varieties of other related meta-information like sample condition (health/disease), cell type, tissue type, sequencing platform, etc. These rich annotations are biologically meaningful and highly correlated with the expression pattern within a cell. The memory consumption for inference with the xTrimoGene-100M model is approximately 50GB, whose hardware requirement (Nvidia A100 80G GPU) is beyond some academic labs, thus computational or memory-efficient engineering techniques tend to advance the model pre-training and application.

xTrimoGene has been integrated into BioMap’s single-cell analysis platform, functioning as a fundamental and essential model (as depicted in the App. Figure 9). The pre-trained model services have been publicly available. In the future, with the increase of data, larger pre-trained models are expected to drive more advancements in various downstream task learning.

Author Contributions and Acknowledgments

Le Song led the project by designing its scope, conceptualizing ideas, integrating resources, and making decisions on techniques. Xingyi Cheng played a key role in the development of the xTrimoGene framework, auto-discretization and unsupervised objectives, contributing concrete ideas and pseudocode, along with code review. Jing Gong and Mingsheng Hao (Research Intern at BioMap) were primarily responsible for conducting pre-training and downstream experiments, serving as the first authors of the paper. Their work covered areas such as model scaling, cell type annotation, perturbation response prediction, and synergistic drug combinations prediction. Xin Zeng made significant contributions to the code of the xTrimoGene framework, worked with an early performer version, and conducted initial downstream experiments. Chiming Liu oversaw the engineering aspects of the project, including the implementation of the data pipeline and FLOPs computation. Jianzhu Ma, Xuegong Zhang, Taifeng Wang, and Le Song conceived the project and provided invaluable guidance for the project and contributed their expertise in computational biology knowledge. Taifeng Wang also played a pivotal role in pushing for the model’s service implementation. Finally, Jing Gong, Mingsheng Hao, Xingyi Cheng, and Le Song collectively contributed to writing this paper.

In addition, we would like to express our gratitude to the individuals at BioMap who have made contributions to our project. Chenrui Xu and Yucheng Guo played roles in data preprocessing and integration. Zhaoren He’s expertise in data analysis and application greatly enhanced our work, and we deeply appreciate his contributions.

This work was supported by the Ministry of Science and Technology of the People’s Republic of China (2022YFF1203004), the Beijing Municipal Science & Technology Commission and the Administrative Commission of Zhongguancun Science Park(Z221100003522022). And this work was also funded by BioMap.

References

John Jumper, Richard Evans, Alexander Pritzel, Tim Green, Michael Figurnov, Olaf Ronneberger, Kathryn Tunyasuvunakool, Russ Bates, Augustin Žídek, Anna Potapenko, et al. Highly accurate protein structure prediction with alphafold. *Nature*, 596(7873):583–589, 2021.

- Zeming Lin, Halil Akin, Roshan Rao, Brian Hie, Zhongkai Zhu, Wenting Lu, Nikita Smetanin, Robert Verkuil, Ori Kabeli, Yaniv Shmueli, et al. Evolutionary-scale prediction of atomic-level protein structure with a language model. *Science*, 379(6637):1123–1130, 2023.
- Ningyu Zhang, Zhen Bi, Xiaozhuan Liang, Siyuan Cheng, Haosen Hong, Shumin Deng, Jiazhang Lian, Qiang Zhang, and Huajun Chen. Ontoprotein: Protein pretraining with gene ontology embedding. *arXiv preprint arXiv:2201.11147*, 2022.
- Yijia Xiao, Jiezhong Qiu, Ziang Li, Chang-Yu Hsieh, and Jie Tang. Modeling protein using large-scale pretrain language model. *arXiv preprint arXiv:2108.07435*, 2021.
- Nadav Brandes, Dan Ofer, Yam Peleg, Nadav Rappoport, and Michal Linial. ProteinBERT: a universal deep-learning model of protein sequence and function. *Bioinformatics*, 38(8):2102–2110, 02 2022. ISSN 1367-4803.
- Jiayang Chen, Zhihang Hu, Siqi Sun, Qingxiong Tan, Yixuan Wang, Qinze Yu, Licheng Zong, Liang Hong, Jin Xiao, Tao Shen, et al. Interpretable rna foundation model from unannotated data for highly accurate rna structure and function predictions. *bioRxiv*, pages 2022–08, 2022a.
- Ahmad Pesaranghader, Stan Matwin, Marina Sokolova, Jean-Christophe Grenier, Robert G Beiko, and Julie Hussin. deepSimDEF: deep neural embeddings of gene products and gene ontology terms for functional analysis of genes. *Bioinformatics*, 38(11):3051–3061, 05 2022. ISSN 1367-4803.
- Dragomirka Jovic, Xue Liang, Hua Zeng, Lin Lin, Fengping Xu, and Yonglun Luo. Single-cell rna sequencing technologies and applications: A brief overview. *Clinical and Translational Medicine*, 12(3):e694, 2022.
- Geng Chen, Baitang Ning, and Tieliu Shi. Single-cell rna-seq technologies and related computational data analysis. *Frontiers in genetics*, page 317, 2019.
- Sijie Chen, Yanting Luo, Haoxiang Gao, Fanhong Li, Yixin Chen, Jiaqi Li, Renke You, Minsheng Hao, Haiyang Bian, Xi Xi, et al. heca: The cell-centric assembly of a cell atlas. *IScience*, 25(5):104318, 2022b.
- Mengwei Li, Xiaomeng Zhang, Kok Siong Ang, Jingjing Ling, Raman Sethi, Nicole Yee Shin Lee, Florent Ginhoux, and Jinmiao Chen. Disco: a database of deeply integrated human single-cell omics data. *Nucleic acids research*, 50(D1):D596–D602, 2022.
- Mario Flores, Zhentao Liu, Tinghe Zhang, Md Musaddaqui Hasib, Yu-Chiao Chiu, Zhenqing Ye, Karla Paniagua, Sumin Jo, Jianqiu Zhang, Shou-Jiang Gao, et al. Deep learning tackles single-cell analysis—a survey of deep learning for scrna-seq analysis. *Briefings in bioinformatics*, 23(1):bbab531, 2022.
- Christopher Heje Grønbech, Maximillian Fornitz Vording, Pascal N Timshel, Casper Kaae Sønderby, Tune H Pers, and Ole Winther. scVAE: variational auto-encoders for single-cell gene expression data. *Bioinformatics*, 36(16):4415–4422, 05 2020. ISSN 1367-4803.
- Romain Lopez, Jeffrey Regier, Michael B Cole, Michael I Jordan, and Nir Yosef. Deep generative modeling for single-cell transcriptomics. *Nature methods*, 15(12):1053–1058, 2018.
- Mohamed Marouf, Pierre Machart, Vikas Bansal, Christoph Kilian, Daniel S. Magruder, and Stefan Bonn Christian F. Krebs. Realistic in silico generation and augmentation of single-cell rna-seq data using generative adversarial networks. *Nature Communications*, 11(1)(166):786–793, 2020.
- Jingshu Wang, Divyansh Agarwal, Mo Huang, Gang Hu, Zilu Zhou, Chengzhong Ye, and Nancy R Zhang. Data denoising with transfer learning in single-cell transcriptomics. *Nature methods*, 16(9):875–878, 2019.
- Xipeng Qiu, Tianxiang Sun, Yige Xu, Yunfan Shao, Ning Dai, and Xuanjing Huang. Pre-trained models for natural language processing: A survey. *Science China Technological Sciences*, 63(10):1872–1897, 2020.

- Xu Han, Zhengyan Zhang, Ning Ding, Yuxian Gu, Xiao Liu, Yuqi Huo, Jiezhong Qiu, Yuan Yao, Ao Zhang, Liang Zhang, Wentao Han, Minlie Huang, Qin Jin, Yanyan Lan, Yang Liu, Zhiyuan Liu, Zhiwu Lu, Xipeng Qiu, Ruihua Song, Jie Tang, Ji-Rong Wen, Jinhui Yuan, Wayne Xin Zhao, and Jun Zhu. Pre-trained models: Past, present and future. *AI Open*, 2:225–250, 2021. ISSN 2666-6510.
- Dan Hendrycks, Kimin Lee, and Mantas Mazeika. Using pre-training can improve model robustness and uncertainty. In Kamalika Chaudhuri and Ruslan Salakhutdinov, editors, *Proceedings of the 36th International Conference on Machine Learning*, volume 97 of *Proceedings of Machine Learning Research*, pages 2712–2721. PMLR, 09–15 Jun 2019.
- Fan Yang, Wenchuan Wang, Fang Wang, Yuan Fang, Duyu Tang, Junzhou Huang, Hui Lu, and Jianhua Yao. scbert as a large-scale pretrained deep language model for cell type annotation of single-cell rna-seq data. *Nature Machine Intelligence*, 4(10):852–866, 2022.
- Ruochen Jiang, Tianyi Sun, Dongyuan Song, and Jingyi Jessica Li. Statistics or biology: the zero-inflation controversy about scrna-seq data. *Genome Biology*, 23(1):31, Jan 2022. ISSN 1474-760X. doi: 10.1186/s13059-022-02601-5. URL <https://doi.org/10.1186/s13059-022-02601-5>.
- Jiarui Ding, Xian Adiconis, Sean K. Simmons, Monika S. Kowalczyk, Cynthia C. Hession, Nemanja D. Marjanovic, Travis K. Hughes, Marc H. Wadsworth, Tyler Burks, Lan T. Nguyen, John Y. H. Kwon, Boaz Barak, William Ge, Amanda J. Kedaigle, Shaina Carroll, Shuqiang Li, Nir Hacohen, Orit Rozenblatt-Rosen, Alex K. Shalek, Alexandra-Chloé Villani, Aviv Regev, and Joshua Z. Levin. Systematic comparison of single-cell and single-nucleus rna-sequencing methods. *Nature Biotechnology*, 38(6):737–746, Jun 2020. ISSN 1546-1696. doi: 10.1038/s41587-020-0465-8. URL <https://doi.org/10.1038/s41587-020-0465-8>.
- Yury Gorishniy, Ivan Rubachev, and Artem Babenko. On embeddings for numerical features in tabular deep learning. *Advances in Neural Information Processing Systems*, 35:24991–25004, 2022.
- Kaiming He, Xinlei Chen, Saining Xie, Yanghao Li, Piotr Dollár, and Ross Girshick. Masked autoencoders are scalable vision learners. In *Proceedings of the IEEE/CVF conference on computer vision and pattern recognition*, pages 16000–16009, 2022.
- Jared Kaplan, Sam McCandlish, Tom Henighan, Tom B Brown, Benjamin Chess, Rewon Child, Scott Gray, Alec Radford, Jeffrey Wu, and Dario Amodei. Scaling laws for neural language models. *arXiv preprint arXiv:2001.08361*, 2020.
- Tom Brown, Benjamin Mann, Nick Ryder, Melanie Subbiah, Jared D Kaplan, Prafulla Dhariwal, Arvind Neelakantan, Pranav Shyam, Girish Sastry, Amanda Askell, et al. Language models are few-shot learners. *Advances in neural information processing systems*, 33:1877–1901, 2020.
- Grace XY Zheng, Jessica M Terry, Phillip Belgrader, Paul Ryvkin, Zachary W Bent, Ryan Wilson, Solongo B Ziraldo, Tobias D Wheeler, Geoff P McDermott, Junjie Zhu, et al. Massively parallel digital transcriptional profiling of single cells. *Nature communications*, 8(1):14049, 2017.
- Åsa Segerstolpe, Athanasia Palasantza, Pernilla Eliasson, Eva-Marie Andersson, Anne-Christine Andréasson, Xiaoyan Sun, Simone Picelli, Alan Sabirsh, Maryam Clausen, Magnus K Bjursell, David M Smith, Maria Kasper, Carina Ämmälä, and Rickard Sandberg. Single-cell transcriptome profiling of human pancreatic islets in health and type 2 diabetes. *Cell Metab.*, 24(4):593–607, October 2016.
- Feiyang Ma and Matteo Pellegrini. Actinn: automated identification of cell types in single cell rna sequencing. *Bioinformatics*, 36(2):533–538, 2020.
- F Alexander Wolf, Philipp Angerer, and Fabian J Theis. Scanpy: large-scale single-cell gene expression data analysis. *Genome biology*, 19:1–5, 2018.
- C. Domínguez Conde, C. Xu, L. B. Jarvis, D. B. Rainbow, S. B. Wells, T. Gomes, S. K. Howlett, O. Suchanek, K. Polanski, H. W. King, L. Mamanova, N. Huang, P. A. Szabo, L. Richardson, L. Bolt, E. S. Fasouli, K. T. Mahbubani, M. Prete, L. Tuck, N. Richoz, Z. K. Tuong, L. Campos, H. S. Mousa, E. J. Needham, S. Pritchard, T. Li, R. Elmentaite, J. Park, E. Rahmani, D. Chen,

- D. K. Menon, O. A. Bayraktar, L. K. James, K. B. Meyer, N. Yosef, M. R. Clatworthy, P. A. Sims, D. L. Farber, K. Saeb-Parsy, J. L. Jones, and S. A. Teichmann. Cross-tissue immune cell analysis reveals tissue-specific features in humans. *Science*, 376(6594):eab15197, 2022. doi: 10.1126/science.ab15197. URL <https://www.science.org/doi/abs/10.1126/science.ab15197>.
- Patrick Cahan Yuqi Tan. Singlecellnet: A computational tool to classify single cell rna-seq data across platforms and across species. *Cell Systems*, 19(2):207–213, 2019.
- Atray Dixit, Oren Parnas, Biyu Li, Jenny Chen, Charles P Fulco, Livnat Jerby-Arnon, Nemanja D Marjanovic, Danielle Dionne, Tyler Burks, Raktima Raychowdhury, et al. Perturb-seq: dissecting molecular circuits with scalable single-cell rna profiling of pooled genetic screens. *cell*, 167(7):1853–1866, 2016.
- Yusuf Roohani, Kexin Huang, and Jure Leskovec. Gears: Predicting transcriptional outcomes of novel multi-gene perturbations. *BioRxiv*, pages 2022–07, 2022.
- Mohammad Lotfollahi, Anna Klimovskaia Susmelj, Carlo De Donno, Yuge Ji, Ignacio L Ibarra, F Alexander Wolf, Nafissa Yakubova, Fabian J Theis, and David Lopez-Paz. Compositional perturbation autoencoder for single-cell response modeling. *BioRxiv*, 2021.
- Thomas M. Norman, Max A. Horlbeck, Joseph M. Replogle, Alex Y. Ge, Albert Xu, Marco Jost, Luke A. Gilbert, and Jonathan S. Weissman. Exploring genetic interaction manifolds constructed from rich single-cell phenotypes. *Science*, 365(6455):786–793, 2019. doi: 10.1126/science.aax4438. URL <https://www.science.org/doi/abs/10.1126/science.aax4438>.
- Reza Bayat Mokhtari, Tina S Homayouni, Narges Baluch, Evgeniya Morgatskaya, Sushil Kumar, Bikul Das, and Herman Yeger. Combination therapy in combating cancer. *Oncotarget*, 8(23):38022, 2017.
- Kristina Preuer, Richard P I Lewis, Sepp Hochreiter, Andreas Bender, Krishna C Bulusu, and Günter Klambauer. DeepSynergy: predicting anti-cancer drug synergy with Deep Learning. *Bioinformatics*, 34(9):1538–1546, 12 2017. ISSN 1367-4803.
- Jinxian Wang, Xuejun Liu, Siyuan Shen, Lei Deng, and Hui Liu. Deepdds: deep graph neural network with attention mechanism to predict synergistic drug combinations. *Briefings in Bioinformatics*, 23(1):bbab390, 2022.

[Appendix materials]

xTrimoGene: An Efficient and Scalable Representation Learner for Single-Cell RNA-Seq Data

Jing Gong^{1*} Minsheng Hao^{12*} Xingyi Cheng^{1†} Xin Zeng¹
 Chiming Liu¹ JianZhu Ma² Xuegong Zhang² Taifeng Wang¹ Le Song^{13†}

¹ BioMap Research, California, USA

² Tsinghua University, Beijing, China

³ Mohamed bin Zayed University of Artificial Intelligence, Abu Dhabi, UAE

{gongjing, minsheng_2022, xingyi, zengxin, chiming, taifeng, songle}@biomap.com,

{zhangxg, majianzhu}@tsinghua.edu.cn

1 scRNA-seq data collection and processing

Recently, scRNA-seq data is rapidly accumulated and mostly has been uploaded to the Gene Expression Omnibus (GEO) repository (<https://www.ncbi.nlm.nih.gov/geo/>). We collected data from GEO and processed data with a unified pipeline.

Downloading data and preparing raw count matrix. We first search scRNA-seq-related data sets in GEO with multiple keywords, including "scRNA-seq", "single-cell RNA-seq", and "single-cell RNA-seq sequencing". The search processes return a list of GSE ID from different studies. After removing the duplicated GSE ID, we downloaded the particular expression or count matrix. Most of the samples provide a raw count matrix. For samples with normalized expression matrices, we converted the matrix back to a count matrix. The conversion strategy is as follows: the minimal non-zero value in the whole normalized matrix is thought to have raw count 1, then all the other normalized values can be converted by scaling to this minimum value.

Matrix mapping to the reference gene list. After preparing all the count matrices, we mapped the matrix to our reference gene list. We downloaded the human protein-coding gene list (about 19,000) from the HUGO Gene Nomenclature Committee (HGNC, <https://www.genenames.org/download/archive/>), plus common mitochondrial genes, jointly constitute our full reference list ($n = 19,264$). For each count matrix, values of those genes not mapped in the reference list are filled with zero.

Quality control. To filter low-quality samples, we only keep samples with over 200 genes expressed (i.e., expression vector with non-zero value count > 200) for subsequent training and analysis.

Normalization. We followed the standard process in Scanpy (<https://scanpy-tutorials.readthedocs.io/en/latest/pbmc3k.html>) [Wolf et al., 2018] to obtain the normalized expression value. There are two steps: (1) for each sample normalize the library size to 10,000. (2) scale the values into a log space.

In summary, all the scRNA-seq data are collected from the Gene Expression Omnibus (GEO) repository with a keyword searching and data retrieval process. Then the downloaded count matrices are processed with a unified pipeline, including reference gene list mapping, quality control and normalization. In total, we curated about 5 million scRNA-seq data for training. The full data set is randomly split into train, validation and test sets with a ratio of 96:2:2.

*Equal contribution. Mingsheng Hao conducted this work during his internship at BioMap.

†Correspondence to: xingyi@biomap.com, songle@biomap.com.

2 Algorithm workflow

We take the below example to demonstrate the processing flow.

Assume the normalized expression value matrix has 2 cells (with 10 genes) as below:

	G1	G2	G3	G4	G5	G6	G7	G8	G9	G10
C1	0.3	2.1	0	4.5	0	7.3	8.9	0	3.4	2.5
C2	1.1	0	0	3.4	2.3	0.7	0	0	2.9	0

First, we masked a portion of values (including zero and non-zero) and the generated matrix is as:

	G1	G2	G3	G4	G5	G6	G7	G8	G9	G10
C1	[M]	2.1	0	4.5	[M]	7.3	8.9	[M]	3.4	2.5
C2	1.1	[M]	[M]	3.4	2.3	[M]	[M]	0	2.9	0

Then, we filter both the [M] token and zero token for each sample. The resulting matrix is as:

	G1	G2	G3	G4	G5	G6	G7	G8	G9	G10
C1		2.1		4.5		7.3	8.9		3.4	2.5
C2	1.1			3.4	2.3				2.9	

Next, we concatenate the rest tokens sequentially and add the [PAD] tokens to match a max-length sample. In this step, some tokens only appear in one cell, introducing the gene inconsistency between the two samples. The generated matrix is as:

	Column1	Column2	Column3	Column4	Column5	Column6
C1	2.1(G2)	4.5(G4)	7.3(G6)	8.9(G7)	3.4(G9)	2.5(G10)
C2	1.1(G1)	3.4(G4)	2.3(G5)	2.9(G9)	[PAD]	[PAD]

3 Auto-discretization strategy evaluation

To validate the effectiveness of the expression value projection, we conducted an analysis of viewing the weight distribution pattern for continuous values. For each value, the auto-discretization block retrieves bucket embeddings (num=100) and combines them in a weighted manner to represent a targeting value. Different values correspond to a particular weight vector once finished training. Theoretically, close values have a similar weight vector distribution and distant values differ. The results showed that the normalized weight distribution of the close values exhibited smooth transitions and that of the distant values being clearly distinguishable (Figure 1). This supports the conclusion that the auto-discretization strategy effectively represents continuous values with high resolution while preserving relatively rich meaning.

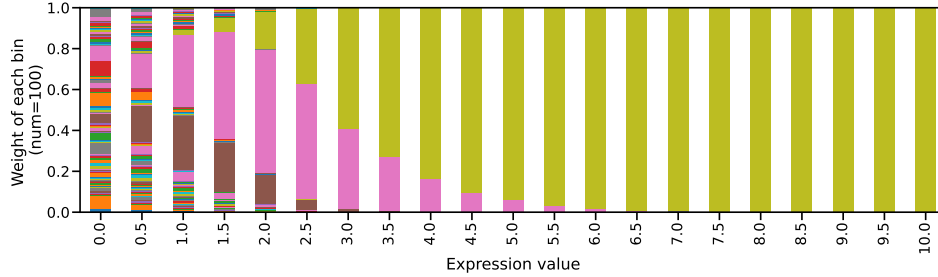


Figure 1: Weight distribution across bins for various expression values. The auto-discretization strategy was applied to each expression value in the range from 0 to 10, producing a corresponding weight vector with a length equal to the number of bins (100 in this case). The weight vectors were normalized to sum to 1 and visualized as stacked plots.

4 Clustering task evaluation and data sets

Cell clustering is an essential task for single-cell research, reflecting the ability of cell embeddings to remove noise and preserve biological signals. In the ablation experiments, we benchmarked the models' clustering performance on two cell-type annotated datasets.

PBMC This dataset is processed by Scanpy python library [Wolf et al., 2018] and contains 2,638 cells. The cell types are annotated by the human with known markers and cover the major immune cells including B cells, CD4 & CD8 T cells, Monocytes, Dendritic cells, Megakaryocytes and NK cells.

Experiments and Evaluation Metric. For every single cell, the expression values are fed into the model and the max pooling layer is applied across all genes' output embedding to get a cell embedding. We then perform the usual single-cell clustering analysis step on these embeddings: 1) build the neighboring graph based on these embeddings and 2) use the Leiden algorithm to cluster the cell into groups. Since the Leiden algorithm requires resolution rather than the number of clusters, we used a dichotomy method to find an optimal resolution reaching the number of cell types given in the dataset.

Several evaluation metrics are applied to access the performance of the clustering results in different aspects, including Adjusted Rand index (ARI), Normalized Mutual Information (NMI), Homogeneity (HOMO), Completeness (CP), and Silhouette Coefficient (SIL). All these metrics are the higher the better. ARI and NMI measure the similarity of the clustering results from the statistics and information entropy theory view, respectively. HOMO and CP are intuitive metrics using conditional entropy analysis. HOMO measures how much the sample in a cluster are similar, and CP measures how much similar samples are put together. SIL measures the similarity of the embeddings to its cluster member compared to other clusters.

5 Acceleration strategy

The attention mechanism in masked language modeling is computationally expensive for long sequences, as time and space complexity grow quadratically along with sequence length. Though multiple attention architectures have been proposed to reduce the complexity to near linear, it's still slow to train large models with billions of data. We have adopted multiple techniques to boost the training speed as follows.

Since FP16 or BFLOAT16 Tensor Core has twice the computational throughput compared to TF32 on NVIDIA Ampere GPU, and, additionally, FP16 training also reduces residual memory consumption, xTrimoGene was conducted mainly with mixed-precision training strategy to optimize computational efficiency.

Distributed Data Parallelism is another training strategy used in our work, which handles large corpus on HPC clusters. In our setting, one single Ampere GPU provides sufficient amounts of memory for one model replica of billions of parameters performing forward and backward passes, and gradient accumulation is used to raise effective batch size to enhance large model training.

To scale up the model size, ZeRO-DP stage two [Rajbhandari et al., 2020] and checkpointing [Chen et al., 2016] techniques are experimentally tested in our setting. The results verified that both strategies reduce the model and residual state memory without expanding training time too much.

For the pre-trained xTrimoGene models, the memory consumption for inference with a sample of approximately 2000 non-zero expressed genes is approximately 50GB for the xTrimoGene-100M model and around 18GB for the xTrimoGene-10M model. It's worth noting that, in line with our pre-training settings, we conducted our tests using bf16 mode on an Nvidia A100 80G GPU. xTrimoGene-100M was trained on 5 million data points across 5 epochs using 64 A100 80G GPUs, with each epoch taking 12 hours.

6 Masking strategy

Table 1: Masking strategy for gene expression matrix. The gene expression matrix is masked by selecting a predetermined number of positions for prediction. $\sim 1,100$ positions, including ~ 600 non-zero and ~ 540 zero expressions, are masked in a matrix with $\sim 20,000$ genes. The performance of the model is evaluated using Mean Squared Error (MSE) loss on these masked positions.

Value	Masked	Unmasked	Total
$\neq 0$	600	1,400	2,000
$= 0$	540	17,460	18,000
sum	1,140 (5.7%)	18,860 (94.3%)	20,000 (100%)

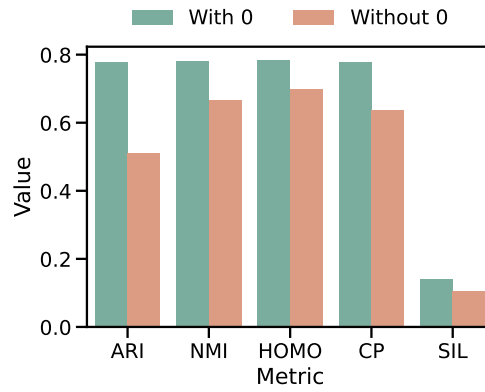


Figure 2: Cell clustering performance for xTrimoGene model considering masking zero (With 0) values or not (Without 0).

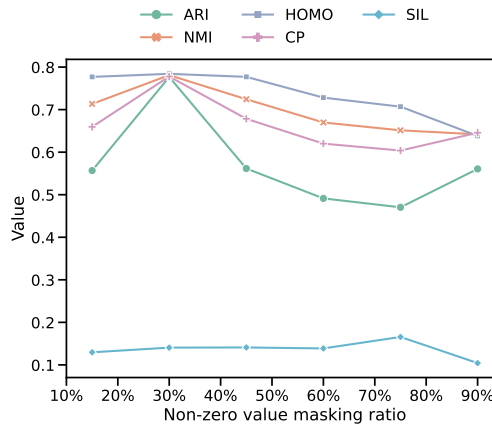


Figure 3: Model performance under different mask ratios of non-zero values. The cell clustering task is evaluated.

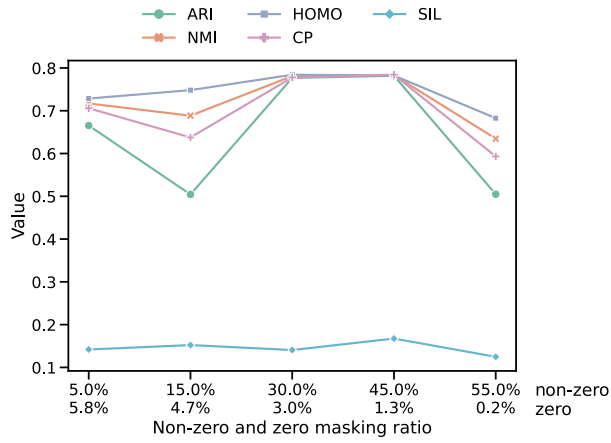


Figure 4: Cell clustering performance for xTrimoGene model with different masking zero, non-zero value ratio.

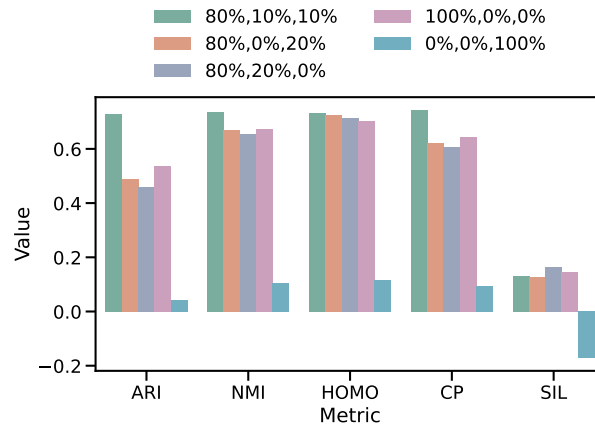


Figure 5: Comparison of performance for xTrimoGene model trained with different masking strategy. percentage1, percentage2, percentage3 denote corresponding replacing probability for three types of tokens: percentage1 for [MASK] token, percentage2 for random expression token and percentage for original token.

7 Scalability

Table 2: Size and hyper-parameters of the pre-trained models. All models are set to train on 5 million data sets and for 5 epochs.

Model name	Parameter (M)	Encoder			Decoder		
		depth	heads	dim	depth	heads	dim
xTrimoGene-3M	3	4	2	128	2	2	128
xTrimoGene-10M	10	4	8	256	2	4	256
xTrimoGene-100M	100	12	12	768	6	8	512

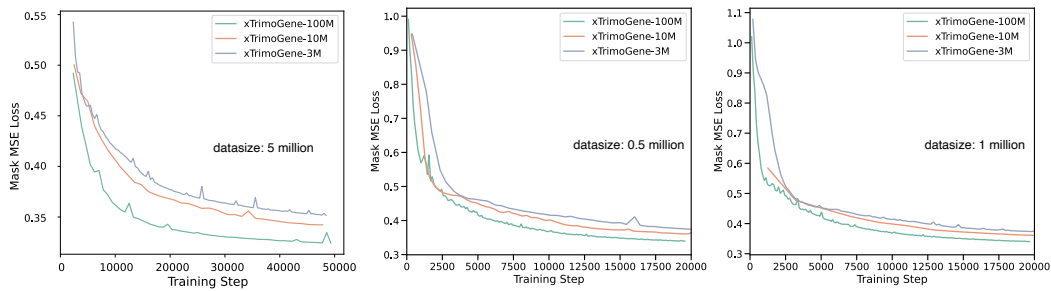


Figure 6: The learning curve of pre-trained xTrimoGene models with different parameter scale. The loss curve measures MSE for masked positions during the pre-training stage, and only the validation set is displayed.

8 Evaluation on downstream tasks

8.1 Cell type annotation task

We downloaded the Zheng68K expression matrix dataset from [Zheng et al., 2017] and the Segerstolpe dataset from [Segerstolpe et al., 2016] and mapped the matrix to our reference gene list. Then, the dataset is split into training, validation and test sets with a ratio of 8:1:1. All the methods are trained on the training set and the best model is selected according to the performance on the validation set. Evaluation metrics (macro F1-score and Marco precision) are calculated for individual testing sets.

In the training process, the expression matrix is fed into the encoder of the xTrimoGene model and the gene embedding is obtained. Then we used a max-pooling layer to aggregate all gene embeddings into one cell embedding, and used a single linear layer to predict cell types from the embeddings.

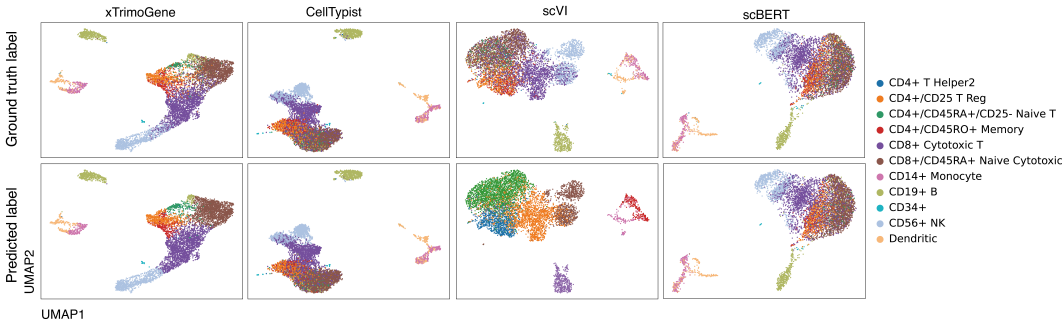


Figure 7: UMAP visualization of different models on the cell type annotation task (Zheng68K dataset). The dot in each panel denotes a cell that is colored by cell type. The two rows denote the ground truth and predicted cell type label, respectively.

8.2 Perturbation effect prediction

The Norman dataset is downloaded from a previous study [Roohani et al., 2022]. The expression matrix data is mapped to our reference gene list. We reproduced the results of GEARS with original codes and settings (<https://github.com/snap-stanford/GEARS>). All the data processing is the same as GEARS, including data split, pre-post sample pairing strategy and evaluation metrics calculation.

While training GEARS with xTrimoGene, the expression matrix is fed into xTrimoGene and intermediate context embedding is obtained. The context embedding is then input to the co-expression graph network branch, all the other parts remain unchanged.

Table 3: The MSE of the top 20 differentially expressed (DE) genes given by different pre-trained models on perturbation response prediction.

Pre-trained model	Total	1-gene	2-gene(seen0)	2-gene(seen1)	2-gene(seen2)
xTrimoGene	0.1983	0.1930	0.2385	0.2100	0.1286
scBERT	0.2231	0.2116	0.2581	0.2386	0.1522

8.3 Drug combination prediction

To test how xTrimoGene adapted to DeepDDS [Wang et al., 2022] for synergistic drug combination prediction, we first reproduced the DeepDDS algorithm. Both data and original codes are downloaded from Github repository (<https://github.com/Sinwang404/DeepDDS/tree/master>). We use data in "new_labels_0.csv" file for training and "independent_set" for testing. The genomic expression data are all mapped to our reference gene list. Models are trained 5 times and evaluated on the testing set. For all metrics, the averaged value and the standard deviation are reported. We keep the

overall framework of DeepDDS while testing xTrimoGene. The genomic expression matrix is fed to xTrimoGene and the intermediate context embedding is obtained. The embedding replaces raw expression profile for MLP branch input.

8.4 Rare cell detection

We also investigate how xTrimoGene behaves on these unseen data, we conduct the following evaluation analysis.

We first collected the scRNA-seq data from a previous study [Ji et al., 2020], which profiles human skin squamous cell carcinoma landscape with scRNA-seq and spatial transcriptomics technology simultaneously. The scRNA-seq data is not present during the xTrimoGene training process. Notably, the authors found that clustering the scRNA-seq data Figure (8, left) yields a novel cell subgroup named TSK (Tumor-Specific Keratinocyte), which is clearly in the tumor sample but not the normal sample.

We employed the tumor scRNA-seq data to explore whether xTrimoGene is robust to distinguish the cell subpopulations from others. The expression matrix is fed into xTrimoGene and the dumped context embedding is used for subsequent UMAP visualization. The results show that the TSK subgroup is clearly separated in Figure (8, right). More importantly, the two TSK subgroups are merged with xTrimoGene, demonstrating its generalization ability to generate good cell-specific embeddings for unseen data.

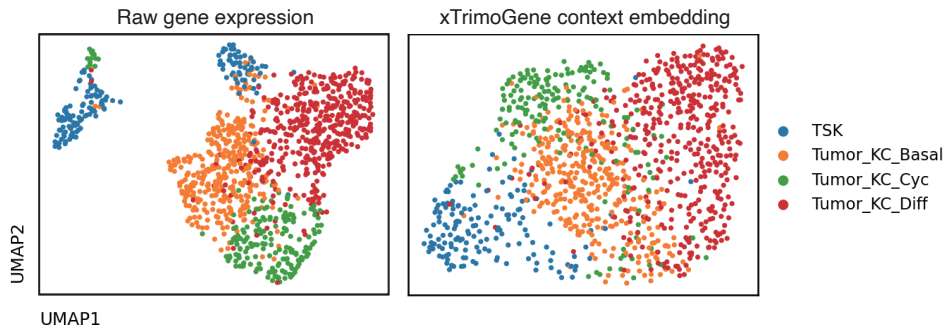


Figure 8: UMAP visualization of tumor scRNA-seq data with a novel TSK subpopulation [Ji et al., 2020]. The left panel denotes dimension reduction with raw normalized gene expression values, while the right panel with xTrimoGene dumped context embedding.

9 Website deployment of xTrimoGene model

xTrimoGene has been proven advantageous in gene representation and cell context embedding extraction. To facilitate its wide application for single-cell RNA-seq data analysis, we deployed the xTrimoGene model within the BioMap corporation. On the website, the xTrimoGene is implemented as a standard operator and serves multiple downstream tasks, including cell clustering, dimension reduction and batch removal Figure (9). The interactive page is user-friendly and feasible to evaluate performance with rich visualizations.

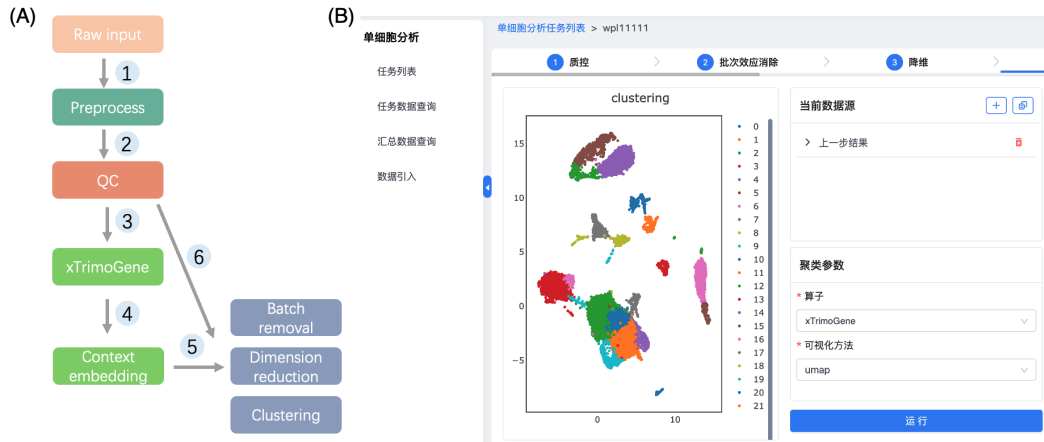


Figure 9: The deployment of xTrimoGene on a website is depicted in this figure. Figure A shows the overall pipeline, which includes the following steps: (1) User-uploaded raw input undergoes preprocessing and filtration through (2) quality control, (3) feeding the processed data into xTrimoGene for (4) context embedding extraction. The model supports multiple downstream applications such as (5) cell clustering, dimension reduction, and batch removal. The extracted expression profile can also be directly utilized by other algorithms. Figure B provides a snapshot of a clustering task in action using xTrimoGene's context embeddings.

References

- F Alexander Wolf, Philipp Angerer, and Fabian J Theis. Scanpy: large-scale single-cell gene expression data analysis. *Genome biology*, 19:1–5, 2018.
- Samyam Rajbhandari, Jeff Rasley, Olatunji Ruwase, and Yuxiong He. Zero: Memory optimizations toward training trillion parameter models. ArXiv, May 2020.
- Tianqi Chen, Bing Xu, Chiyuan Zhang, and Carlos Guestrin. Training deep nets with sublinear memory cost. *CoRR*, abs/1604.06174, 2016.
- Grace XY Zheng, Jessica M Terry, Phillip Belgrader, Paul Ryvkin, Zachary W Bent, Ryan Wilson, Solongo B Ziraldo, Tobias D Wheeler, Geoff P McDermott, Junjie Zhu, et al. Massively parallel digital transcriptional profiling of single cells. *Nature communications*, 8(1):14049, 2017.
- Åsa Segerstolpe, Athanasia Palasantza, Pernilla Eliasson, Eva-Marie Andersson, Anne-Christine Andréasson, Xiaoyan Sun, Simone Picelli, Alan Sabirsh, Maryam Clausen, Magnus K Bjursell, David M Smith, Maria Kasper, Carina Ämmälä, and Rickard Sandberg. Single-cell transcriptome profiling of human pancreatic islets in health and type 2 diabetes. *Cell Metab.*, 24(4):593–607, October 2016.
- Yusuf Roohani, Kexin Huang, and Jure Leskovec. Gears: Predicting transcriptional outcomes of novel multi-gene perturbations. *BioRxiv*, pages 2022–07, 2022.
- Jinxian Wang, Xuejun Liu, Siyuan Shen, Lei Deng, and Hui Liu. Deepdds: deep graph neural network with attention mechanism to predict synergistic drug combinations. *Briefings in Bioinformatics*, 23(1):bbab390, 2022.
- Andrew L. Ji, Adam J. Rubin, Kim Thrane, Sizun Jiang, David L. Reynolds, Robin M. Meyers, Margaret G. Guo, Benson M. George, Annelie Mollbrink, Joseph Bergensträhle, Ludvig Larsson, Yunhao Bai, Bokai Zhu, Aparna Bhaduri, Jordan M. Meyers, Xavier Rovira-Clavé, S. Tyler Hollmig, Sumaira Z. Aasi, Garry P. Nolan, Joakim Lundeberg, and Paul A. Khavari. Multimodal analysis of composition and spatial architecture in human squamous cell carcinoma. *Cell*, 182(2):497–514.e22, 2020. ISSN 0092-8674. doi: <https://doi.org/10.1016/j.cell.2020.05.039>. URL <https://www.sciencedirect.com/science/article/pii/S0092867420306723>.